Doctorate of Philosophy

Schrödinger's Catwalk

Brian Flynn

University of Bristol

November, 2020

CONTENTS

LIST OF TABLES

LIST OF FIGURES

LISTINGS

ACRONYMS

BF	Bayes factor. 2, 11
EDH	experiment design heuristic. 7, 8
ES	exploration strategy. 2, 11, 16
FH	Fermi-Hubbard. 9
QHL	quantum Hamiltonian learning. 5, 7, 8, 16
QMLA	Quantum Model Learning Agent. i, 2, 3, 11, 16

GLOSSARY

Jordan Wigner transformation (JWT)	Jordan Wigner transformation . 10
instance	a single implementation of the QMLA algorithm. 16
probe	Input probe state, $\|\psi\rangle$, which the target system is initialised to, before unitary evolution. plural. 5
run	collection of QMLA instances. 16
volume	Volume of a parameter distribution's credible region.. 6–8

Part I

THEORETICAL STUDY

1 PRESCRIBED MODEL SETS

A sensible first case study for the QMLA framework is to prescribe a set of models, where we know that the true model is among them, or at least that we would be satisfied with approximating $\hat{H}_0$ as the best model in the set. This application can be useful, for example, for expedited device calibration; suppose we wish to characterise a new, untrustued quantum simulator/device, S_u, and we have access to a *trusted*[1] simulator, S_t. In order to perform this calibration, we treat S_u as the system, Q, i.e. we call upon it to retrieve the datum d in **??**, where the calculation of the likelihoods for each particle are computed through S_t. If S_u is reliable, the data from its calculations will be consistent with some $\hat{H}_0$ of our choosing, while miscalibrations will mainfest as imperfectly implemented gates/steps in the calculation of the system's likelihood, and so would result in data inconsistent with $\hat{H}_0$. Therefore, if we can prescribe the most likely miscalibrations, it may be feasible to compose a set of models, $\mathbb{H}$, which represent those cases, and search for $\hat{H}'$ only within $\mathbb{H}$, to find identify the miscalibrations. For example, by encoding connections between every pair of device qubits in $\hat{H}_0$, we can compose models with restricted connectivity, for instance where some pairs of qubits are disconnected, and hence discover whether the device allows arbitrary two-qubit gates, and which pairs are disallowed.

1.1 LATTICES

We first consider Q as some lattice, where QMLA attempts to identify the structure of the lattice. The set of viable models then comprises alternative lattices. Due to simluation constraints, because we train models through exact unitary evolution, we are restricted to $\sim$ 8-qubit Hamiltonians, so we only consider lattices which can be simulated in this limit. The ES in this chapter is then simply to propose a set of models with no further model generation, with comparisons between all pairs of models through Bayes factors (BFs).

Connectivity between lattice sites is achieved within the specific Hamiltonian formalisms introduced in the following sections, although in general we write $\mathcal{C} = \{\langle k, l \rangle\}$ as the set of connected pairs $\langle k, l \rangle$, such that the Hamiltonian for a given lattice can be thought of as some function of its configuration, $\hat{H}(\vec{\alpha}, \mathcal{C})$. Then, we can specify candidate models only by their $\mathcal{C}$, e.g. a 3-site chain can be summarised by $\mathcal{C} = \{\langle 1,2 \rangle, \langle 2,3 \rangle\}$, whereas a fully connected 3-site lattice (i.e. a triangle) is given by $\mathcal{C} = \{\langle 1,2 \rangle, \langle 1,3 \rangle, \langle 2,3 \rangle\}$. We can then summarise the set of candidate models through the descriptions of lattice configurations, corresponding to those depicted in Fig. 1.1:
a. 2-site chain

1 Note: here a classical computer can fulfil the role of the trusted simulator.

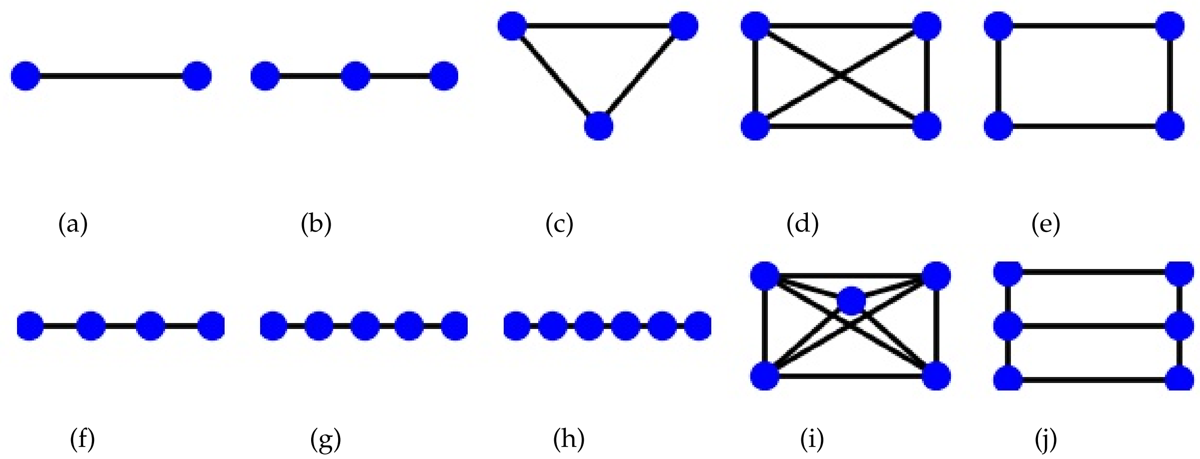

Figure 1.1: Lattices used for prescribed models test for QMLA. Lattices are characterised by the connectivity of their sites; dotted lines show connection between pairs of sites.

b. 3-site chain
c. 3-site fully connected (triangle)
d. 4-site fully conneted (square)
e. 4-site linearly connected (loop)
f. 4-site chain
g. 5-site chain
h. 6-site chain
i. 5-site fully connected (pentagon)
j. 6-site partially connected (grid)

We will use this set of lattice configurations throughout the remainder of this chapter.

1.2 ISING MODEL

The Ising model is one of the most studied concepts in all of physics, representing electrons on a lattice of N sites, where each electron can have *spin* up or down [1, 2, 3]. Interactions between spins $\langle k, l \rangle$ have strength J_{kl}, and the transverse magnetic field acts on spin k with strength h_k. It is usually stated as

$$\hat{H}_I(\mathcal{C}) = \sum_{\langle k,l \rangle \in \mathcal{C}} J_{kl} \, \hat{\sigma}_k^z \, \hat{\sigma}_l^z + \sum_{k=1}^{N} h_k \hat{\sigma}_k^x. \tag{1.1}$$

The interaction term indicates the class of magnetism of the pair's interaction, i.e.

$$\begin{cases} J_{kl} < 0, & \text{ferromagnetic;} \\ J_{kl} > 0, & \text{antiferromagnetic;} \\ J_{kl} = 0, & \text{noninteracting.} \end{cases} \tag{1.2}$$

If all interaction pairs are described by the same case in Eq. (1.2), the entire system can be said belong to that class of magnetism.

1.2.1 *Note on optimising the Ising model*

Many treatments of the Ising model seek to find the ground state of the system by optimising the configuration of spins in the system. This involves neglecting the transverse magnetic field, and treating Ising model classically, such that the ground state is found by minimising the energy function

$$E_I = \langle \psi | H_I | \psi \rangle = \sum_{\langle k,l \rangle \in \mathcal{C}} J_{kl} \ \langle \psi | \hat{\sigma}_k^z \, \hat{\sigma}_l^z | \psi \rangle \,, \tag{1.3}$$

where $|\psi\rangle = |\psi_1\rangle \otimes |\psi_2\rangle \cdots \otimes |\psi_N\rangle$.

This optimisation relies on the relationship between the Ising model with its eigenvalues and eigenstates: Eq. (1.3) consists only of $\hat{\sigma}^z$ terms, and we have that

$$\hat{\sigma}^z \, |+\rangle = +1 \, |+\rangle \quad ; \quad \hat{\sigma}^z \, |-\rangle = -1 \, |-\rangle \,. \tag{1.4}$$

Then, for a single pair of spins $\langle k, l \rangle$, we have

$$\begin{aligned} \langle +_k \, +_l | \, \hat{\sigma}_k^z \, \hat{\sigma}_l^z \, | +_k \, +_l \rangle &= \langle +_k \, +_l | \, (+1)(+1) \, | +_k \, +_l \rangle = +1, \\ \langle +_k \, -_l | \, \hat{\sigma}_k^z \, \hat{\sigma}_l^z \, | +_k \, -_l \rangle &= \langle +_k \, -_l | \, (+1)(-1) \, | +_k \, -_l \rangle = -1, \\ \langle -_k \, +_l | \, \hat{\sigma}_k^z \, \hat{\sigma}_l^z \, | -_k \, +_l \rangle &= \langle -_k \, +_l | \, (-1)(+1) \, | -_k \, +_l \rangle = -1, \\ \langle -_k \, -_l | \, \hat{\sigma}_k^z \, \hat{\sigma}_l^z \, | -_k \, -_l \rangle &= \langle -_k \, +_l | \, (-1)(1) \, | -_k \, -_l \rangle = +1. \end{aligned} \tag{1.5}$$

So, by restricting the individual spins to $|\psi_k\rangle \in \{|+\rangle, |-\rangle\}$, we can equivalently consider every spin s_k in the system as a binary variable $s_k \in \{\pm 1\}$, i.e. $s_k s_l = \pm 1$ in Eq. (1.5), such that the energy function

$$E_I(\mathcal{S}) = \langle \psi | \hat{H}_I | \psi \rangle = \sum_{\langle k,l \rangle \in \mathcal{C}} J_{kl} \ \ s_k s_l \tag{1.6}$$

can be minimised by optimising the configuration $\mathcal{S}$, when the interaction terms $\{J_{\langle k,l \rangle}\}$ are known. The optimal configuration $\mathcal{S}_0$ can then be mapped to a state vector $|\psi_0\rangle$, i.e. the ground state of the system.

While this task can be greatly simplified by the reduction in Eq. (1.5), meaning we do not have to compute any unitary evolution to evaluate Eq. (1.6), it is still an expensive optimisation, because effectively it is a search over $\{|\psi\rangle\}$, so the search space has 2^N candidates [2, 4]. This allows for a straightforward mapping between ground state search and solving combinatorial optimsiation algorithms, namely MAX-CUT, known to be NP-complete [5], allowing for proposed advantage in mapping computationally challenging problems to quantum hardware [6]. This mapping underlies ongoing research into quantum annealing as a computational platform capable of providing advantage for a specific family of problems [7, 8, 9].

Crucially, our goal is *not* to find the ground state of Q, but instead to find the generator of its dynamics. Therefore, we treat the Ising *quantum mechanically*: instead of treating Eq. (1.1) as the underlying mechanism for a cost function to be optimised, i.e. Eq. (1.6), we use quantum operators and do not necessarily restrict the probe state $|\psi\rangle$, allowing us to use Eq. (1.1) within the likelihood function **??**.

1.2.2 *Ising model cases*

We consider two cases: firstly, where it is assumed that the strength of interactions $J_{k,l}$ are uniform (given by J); and secondly, where each interaction is assigned a unique parameter (J_{kl}). In the first case, we can represent the Ising model for a given lattice configuration $\mathcal{C}$ as

$$\hat{H}(\mathcal{C}) = J \sum_{\langle k,l \rangle \in \mathcal{C}} \hat{\sigma}_k^z \hat{\sigma}_l^z + h \sum_{k=1}^{N} \hat{\sigma}_k^x, \tag{1.7}$$

allowing for the compact representation, following **??**,

$$\vec{\alpha}_I = \begin{pmatrix} J & h \end{pmatrix} \tag{1.8a}$$

$$\vec{T}_I = \begin{pmatrix} \sum\limits_{\langle k,l \rangle \in \mathcal{C}} \hat{\sigma}_k^z \hat{\sigma}_l^z \\ \sum\limits_{k=1}^{N} \hat{\sigma}_k^x \end{pmatrix}. \tag{1.8b}$$

In the more general second case, termed the *fully parameterised* Ising model, we instead have the term set

$$\mathcal{T}_I = \left\{ \hat{\sigma}_k^z \hat{\sigma}_l^z, \ \sum_{k=1}^{N} \hat{\sigma}_k^x \right\}_{\langle k,l \rangle \in \mathcal{C}}. \tag{1.9}$$

with unique parameters J_{kl} associated with each interaction term $\hat{\sigma}_k^z \hat{\sigma}_l^z$. We summarise these cases in Table 1.1.

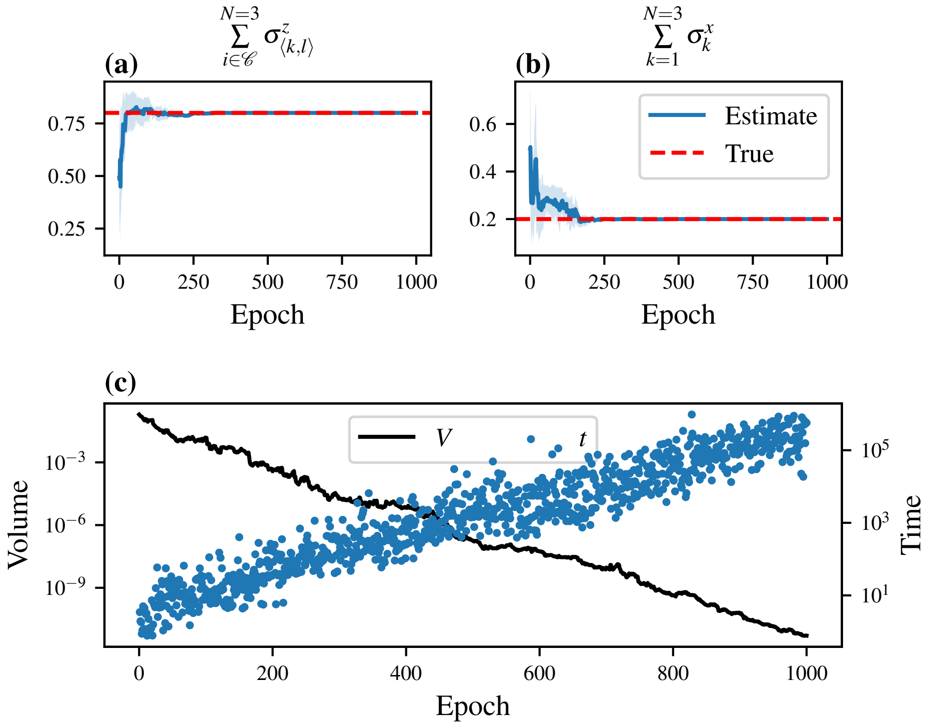

Figure 1.2: QHL for Ising model where terms are grouped by their functionality, as in Eq. (1.1). (a,b) show the parameter estimates progression against epochs (experiments), with the corresponding term written on top of the plot; (c) shows the volume of the parameter distribution at each epoch, as well as the evolution time chosen by the experiment design heuristic (EDH). Implementation details are listed in Table A.1

	$J_{\langle k,l\rangle}$	h_k
Standard	J	h
Fully parameterised	$J_{\langle k,l\rangle}$	h_k

Table 1.1: Types of Ising model. Varying whether parameters $J^z_{\langle k,l\rangle}, h_k$ are shared across sites gives distinct models.

We first construct models under each of these forms to verify QHL is capable of learning in this regime. The former case is the standard form of the Ising model; its training is shown in Fig. 1.2, while the fully paramterised model is shown in Fig. 1.3. Ultimately, these two cases give the same Hamiltonian when $J_{\langle k,l\rangle} = J$; $h_k = h\ \forall k, l$. So, the fully parameterised model will learn the same parameters as the standard Ising model, and we can take the BF between them to determine which parameterisation is favourable. Encouragingly, both models learaned the parameters to high precision, and neither model converged; the volume continues to reduce

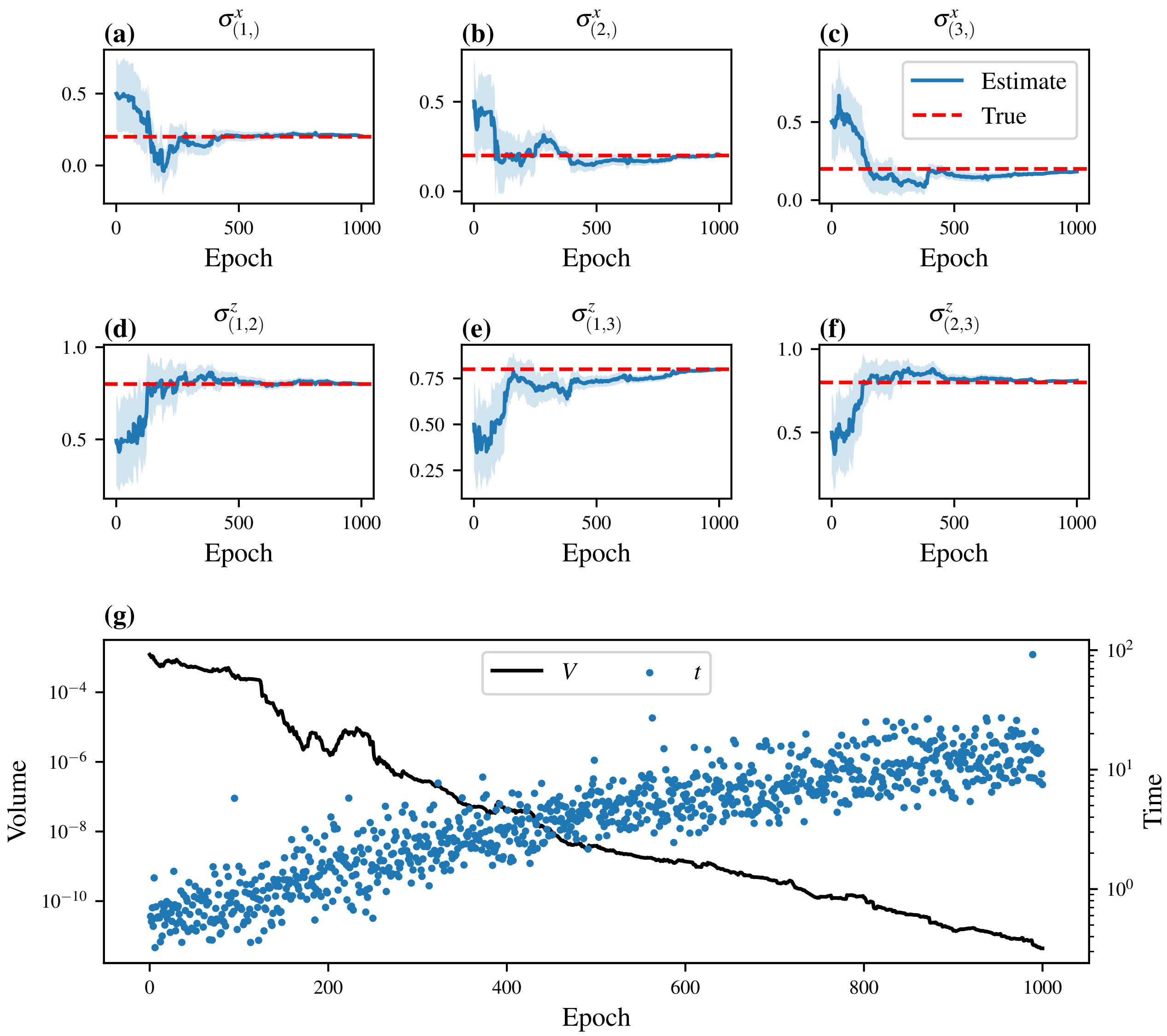

Figure 1.3: QHL for fully parameterised Ising model, where every interaction between pairs of sites are assigned unique parameters, here neglecting the transverse field, as in Eq. (1.9). (a)-(f) show the parameter estimates progression against epochs (experiments), with the corresponding term written on top of the plot; (g) shows the volume of the parameter distribution at each epoch, as well as the evolution time chosen by the EDH. Implementation details are listed in Table A.1

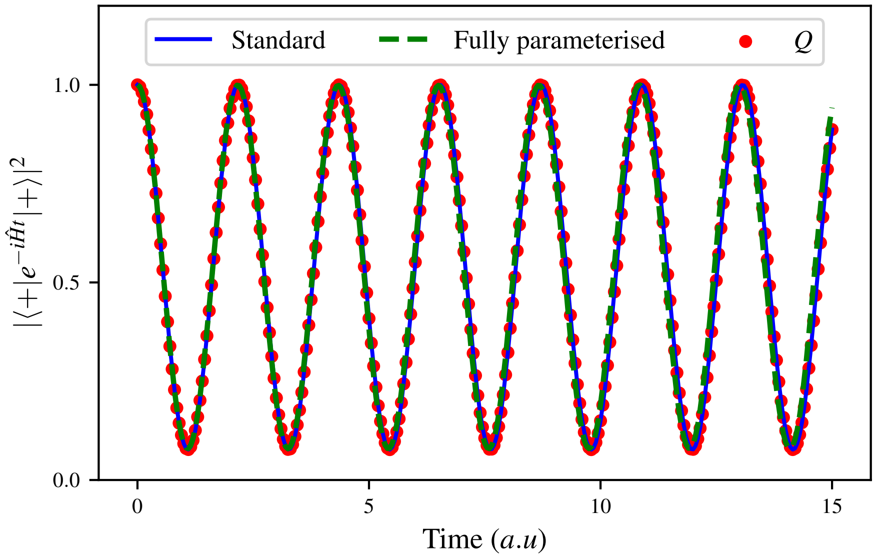

Figure 1.4: Dynamics reproduced by Ising models under standard and fully parameterised formalisms, compared with dynamics for the true system. Implementation details are listed in Table A.1

exponentially in both cases, suggesting it may be impractical to seek saturation in the model training phase for every model, since this may require a very large number of experiments and particles.

The dynamics produced by both models are shown in Fig. 1.4: the dynamics are almost indistinguishable by eye, but the standard Ising model, which in this case is $\hat{H}_0$, outperforms the fully parameterised model, by a BF of 10^{19}. This serves as a good *sanity check*, confirming our expectation that the BF will favour the simpler model (i.e. fewer parameters) even when both models are trained to a high precision to very similar parmaeters, and are difficult to distinguish through human intuition.

1.3 HEISENBERG MODEL

Generalising the Ising model, the Heisenberg Hamiltonian is another model for magnetic systems consisting of a set of spins on a lattice [10]. It builds on the Ising model by additionally considering the spins' rotations about the $x-$ and $y-$ axes, generally stated as

$$\hat{H}_H(\mathcal{C}) = \sum_{\langle k,l\rangle \in \mathcal{C}} J^x_{kl}\ \hat{\sigma}^x_k \hat{\sigma}^x_l + \sum_{\langle k,l\rangle \in \mathcal{C}} J^y_{kl}\ \hat{\sigma}^y_k \hat{\sigma}^y_l + \sum_{\langle k,l\rangle \in \mathcal{C}} J^z_{kl}\ \hat{\sigma}^z_k \hat{\sigma}^z_l + \sum_{k=1}^{N} h_k \hat{\sigma}^z_k. \tag{1.10}$$

We can consider a number of formulations of the Heisenberg model, by considering whether the interaction parameters are completely unique for each pair of spins in each axis, or are shared by pairs of spins; we list the instances within the family of Heisenberg models in Table 1.2.

	J^x_{kl}	J^y_{kl}	J^z_{kl}	h_k
XXX	J^x	J^x	J^x	h
XXZ	J^x	J^x	J^z	h
XYZ (standard)	J^x	J^y	J^z	h
Fully parameterised	J^x_{kl}	J^y_{kl}	J^z_{kl}	h_k

Table 1.2: Heisenberg model types: varying whether the interaction parameters J^w_{kl} are shared among pairs of spins give distinct descriptions which are all in the family of Heisenberg models.

Again, there are a number of possibile models to test, although we can reasonably expect these to follow the same arguments as for the Ising model cases: increasing generality at the expense of larger parameter dimension requires more resources to learn to a reasonable level. In this chapter we will refer to the Heisenberg-XYZ model, and will consider the fully parameterised Heisenberg model in Chapter 3; the parameters and terms of interest are then captured by Eq. (1.11).

$$\vec{\alpha}_H = \begin{pmatrix} J^x & J^y & J^z & h \end{pmatrix} \tag{1.11a}$$

$$\vec{T}_H = \begin{pmatrix} \sum\limits_{\langle k,l \rangle \in \mathcal{C}} \hat{\sigma}^x_k \hat{\sigma}^x_l \\ \sum\limits_{\langle k,l \rangle \in \mathcal{C}} \hat{\sigma}^y_k \hat{\sigma}^y_l \\ \sum\limits_{\langle k,l \rangle \in \mathcal{C}} \hat{\sigma}^z_k \hat{\sigma}^z_l \\ \sum\limits_{k=1}^{N} \hat{\sigma}^z_k \end{pmatrix} \tag{1.11b}$$

1.4 HUBBARD MODEL

Another representation of solid state matter systems is given by the Hubbard model [11, 12, 13]. The Hubbard model deals with systems of correlated fermions, allowing spins to *hop* between sites. Note the Hubbard model is synonymous with the Fermi-Hubbard (FH) model, which can be used to distinguish this model of fermions from a similar model of bosons, named the Bose-Hubbard model, which is not studied in this thesis. We use the subscript FH to distinguish the (Fermi-)Hubbard model from the Heisenberg model $\hat{H}_H$, Eq. (1.10). The Hubbard model is generally stated in second quantisation as

$$\hat{H}_{FH}(\mathcal{C}) = \sum_{s\in\{\uparrow,\downarrow\}} \sum_{\langle k,l\rangle\in\mathcal{C}} t^s_{\langle k,l\rangle} \left(\hat{c}^\dagger_{ks}c_{ls} + \hat{c}^\dagger_{ls}c_{ks}\right) + \sum_k^N U_k \hat{n}_{k\uparrow}\hat{n}_{k\downarrow} + \sum_k^N \mu_k \left(\hat{n}_{k\uparrow} + \hat{n}_{k\downarrow}\right) \tag{1.12}$$

where

- $\hat{c}_{ks}$ and $\hat{c}^\dagger_{ks}$ are respecitvely the fermionic annihilation and creation operators for spin $s \in \{\uparrow,\downarrow\}$ on site k;
- $\hat{n}_{ks} = \hat{c}^\dagger_{ks}\hat{c}_{ks}$ is a counting operator to count the number of spins s on site k;
- $t^s_{\langle k,l\rangle}$ is the kinetic (hopping) term for spin s between sites k and l;
- U_k is the onsite (repulsion) energy for site k;
- μ_k is the chemical energy for k;
- N is the number of sites in the system.

Again, we can achieve differing physics by controlling whether the parameters are shared, with similar consequences to the Ising and Heisenberg models, where additional parameterisation comes at the expense of slower/worse performance in training. We list a subset of possible configurations in Table 1.3; we will use the standard form in this chapter, i.e.

$$\vec{\alpha}_{FH} = \begin{pmatrix} t^\uparrow & t^\downarrow & U & \mu \end{pmatrix} \tag{1.13a}$$

$$\vec{T}_{FH} = \begin{pmatrix} \sum\limits_{\langle k,l\rangle\in\mathcal{C}} \left(\hat{c}^\dagger_{k,\uparrow}\hat{c}_{l,\uparrow} + \hat{c}^\dagger_{l,\uparrow}\hat{c}_{k,\uparrow}\right) \\ \sum\limits_{\langle k,l\rangle\in\mathcal{C}} \left(\hat{c}^\dagger_{k,\downarrow}\hat{c}_{l,\downarrow} + \hat{c}^\dagger_{l,\downarrow}\hat{c}_{k,\downarrow}\right) \\ \sum\limits_{k=1}^N \hat{n}_{k\uparrow}\hat{n}_{k\downarrow} \\ \sum\limits_{k=1}^N \left(\hat{n}_{k\uparrow} + \hat{n}_{k\downarrow}\right) \end{pmatrix} \tag{1.13b}$$

	$t^\uparrow_{\langle k,l\rangle}$	$t^\uparrow_{\langle k,l\rangle}$	U_k	μ_k
Standard	$t^\uparrow$	$t^\downarrow$	U	μ
Fully parameterised	$t^\uparrow_{\langle k,l\rangle}$	$t^\downarrow_{\langle k,l\rangle}$	U_k	μ_k

Table 1.3: Types of Hubbard model. Varying whether parameters $t^s_{\langle k,l\rangle}, U_k, \mu_k$ are shared across sites gives distinct models.

1.4.1 *Jordan Wigner transformation*

In order that the Hubbard model is simulateable with qubits[2], it must first undergo a mapping from the fermionic representation to a spin system representation; such a mapping is given by the Jordan Wigner transformation (JWT) [14, 15]. We implement the JWT within QMLA through OpenFermion's fermilib package [16].

In second quantisation, the fermions on the lattice can occupy one (or a superposition of) *modes*, for example, spin $\uparrow$ on the site indexed 3 is a mode. The system can then be given by a state in the *number basis*,

$$|\psi_f\rangle = |n_{m_1}, n_{m_2}, \dots, n_{m_n}\rangle , \tag{1.14}$$

where n_{m_i} is the number of fermions on mode m_i and there are n modes in total.

$\hat{c}^{\dagger}_{m_i}$ ($\hat{c}_{m_i}$) is the creation (annihilation) operator on the mode m_i: it acts on the system by adding (removing) a fermion from (to) m_i:

$$\hat{c}^{\dagger}_{m_i} |\psi_f\rangle = |n_{m_1}, \dots, n_{m_i} + 1, \dots, n_{m_n}\rangle , \tag{1.15a}$$

$$\hat{c}_{m_i} |\psi_f\rangle = |n_{m_1}, \dots, n_{m_i} - 1, \dots, n_{m_n}\rangle . \tag{1.15b}$$

In the Hubbard model, we assign a mode for each combination of spin $s \in \{\uparrow, \downarrow\}$ with each site k, i.e. the system is in the state

$$|\psi_{FH}\rangle = |n_{1\uparrow}, n_{1\downarrow}, \dots, n_{N\uparrow}, n_{N\downarrow}\rangle . \tag{1.16}$$

In particular, since fermions obey the Pauli exclusion principle, i.e. every spin/site can be occupied by at most one electron, and we can view them as two-level systems, so we have $n_{sk} \in \{0, 1\} \forall s, k$, We therefore use a similar system to the number basis: a qubit registered as $|0\rangle$ corresponds to an empty mode, while $|1\rangle$ holds a fermion. Empty lattices are thus given by $|0\rangle^{\otimes 2N}$. Then, in analogue with the annihilation and creation operators, we introduce oeprators $\hat{\sigma}^{+}, \hat{\sigma}^{-}$ such that

$$\hat{\sigma}^{+} = \begin{pmatrix} 0 & 0 \\ 1 & 0 \end{pmatrix} \implies \hat{\sigma}^{+} |0\rangle = |1\rangle \tag{1.17a}$$

$$\hat{\sigma}^{-} = \begin{pmatrix} 0 & 1 \\ 0 & 0 \end{pmatrix} \implies \hat{\sigma}^{-} |1\rangle = |0\rangle \tag{1.17b}$$

Then, to map the number basis of Eq. (1.16) to a state which can be prepared on qubits, the JWT assigns a single qubit to each mode, where qubits are ordered simply by the site index and spin type, as shown in Table 1.4. The JWT can be summarised by mapping – for the mode m – the

2 Or simulations of qubits, as in this thesis.

Mode	Site	Spin	Qubit
1	1	$\uparrow$	1
2	1	$\downarrow$	2
3	2	$\uparrow$	3
4	2	$\downarrow$	4
	$\vdots$		
$2N-1$	N	$\downarrow$	$2N-1$
$2N$	N	$\uparrow$	$2N$

Table 1.4: Jordan Wigner mode/qubit indices.

creation (annihilation) operator $\hat{c}_m^\dagger$ ($\hat{c}_m$), to an operator which adds a spin to the corresponding state through the operator $\hat{\sigma}_m^+$ ($\hat{\sigma}_m^-$).

$$\hat{c}_m \rightarrow (\hat{\sigma}^z)^{\otimes k-1} \otimes \hat{\sigma}^- \otimes (\hat{\sigma}^z)^{\otimes 2N-1} \tag{1.18a}$$

$$\hat{c}_m^\dagger \rightarrow (\hat{\sigma}^z)^{\otimes k-1} \otimes \hat{\sigma}^+ \otimes (\hat{\sigma}^z)^{\otimes 2N-1} \tag{1.18b}$$

Note the JWT acts on all modes/qubits other than the target with $\hat{\sigma}^z$, since

For example, an empty 2-site lattice $|\psi_0\rangle$ is acted on by a creation operator on mode 3, corresponding to spin $\uparrow$ on site 2:

$$\hat{c}_{2\uparrow}^\dagger |0000\rangle = \hat{c}_3^\dagger |0000\rangle = \hat{\sigma}_1^z \hat{\sigma}_2^z \hat{\sigma}_3^+ \hat{\sigma}_4^z |0000\rangle = |0010\rangle \tag{1.19}$$

1.4.2 *Half filled basis*

In principle there can be $2N$ spins on a lattice of N sites, although in general we will restrict to the case where there are N spins in the lattice, known as *half-filling*, such that Eq. (1.16) is effectively projected into the subspace spanned by half-filled basis states. For example, with $N = 2$

$$\{|1100\rangle, |1010\rangle, |1001\rangle, |0101\rangle, |0110\rangle, |0011\rangle\} \tag{1.20}$$

Therefore, in the design of probes for training Hubbard models, we can generate probes in the subspace spanned by half-filled states.

1.5 MODEL LEARNING FOR LATTICES

Finally, then, we can use the lattice systems introduced in Sections 1.1 to 1.4 as first case studies for QMLA. Each $\mathcal{C} \in \mathbb{C}$ can specify a unique model under the standard model formalism for each of Ising (Eq. (1.8)), Heisenberg (Eq. (1.11)) and Hubbard (Eq. (1.13)) models. We can then devise a simple ES which only tests the models corresponding to $\mathbb{C}$, with no further model generation, i.e. Algorithm 1, and compares every pair of models through BF, deeming the champion as that which wins the largest number of comparisons, as in Algorithm 2.

Algorithm 1: Lattice exploration strategy: model generation

```
Input: ℂ                                              // Set of lattice configurations
Output: {Ĥ_i}                                          // Set of models to tests

ℍ = { }
for 𝒞 ∈ ℂ do
  | Ĥ_i ← map_lattice_to_model(𝒞)
  | ℍ ← ℍ ∪ {Ĥ_i}
end
return ℍ
```

Algorithm 2: Lattice exploration strategy: consolidation

```
Input: ℍ                                               // Set of trained models
Output: Ĥ'                                             // Favoured model

for Ĥ_i ∈ ℍ do
  | s_i ← 0                                            // Score for every model
end
for Ĥ_i ∈ ℍ do
  | for Ĥ_j ∈ ℍ \ {Ĥ_i} do
  |   | B_ij ← BF(Ĥ_i, Ĥ_j)                            // Compute Bayes factor via ??
  |   | if B_ij > 1 then
  |   |   | s_i ← s_i + 1          // Ĥ_i's score increases if it is the stronger model
  |   | end
  | end
end
Ĥ' ← argmax_{s_i} (Ĥ_i)
return Ĥ'
```

For example, we adopt the fully connected four site lattice (d in Fig. 1.1) as the true lattice specifying $\hat{H}_0$, under the Ising formalism (Eq. (1.7)). We run QMLA by training the ten models corresponding to the ten lattices, Fig. 1.5**a-b**; comparing the models predictive power, Fig. 1.5**c-d**,

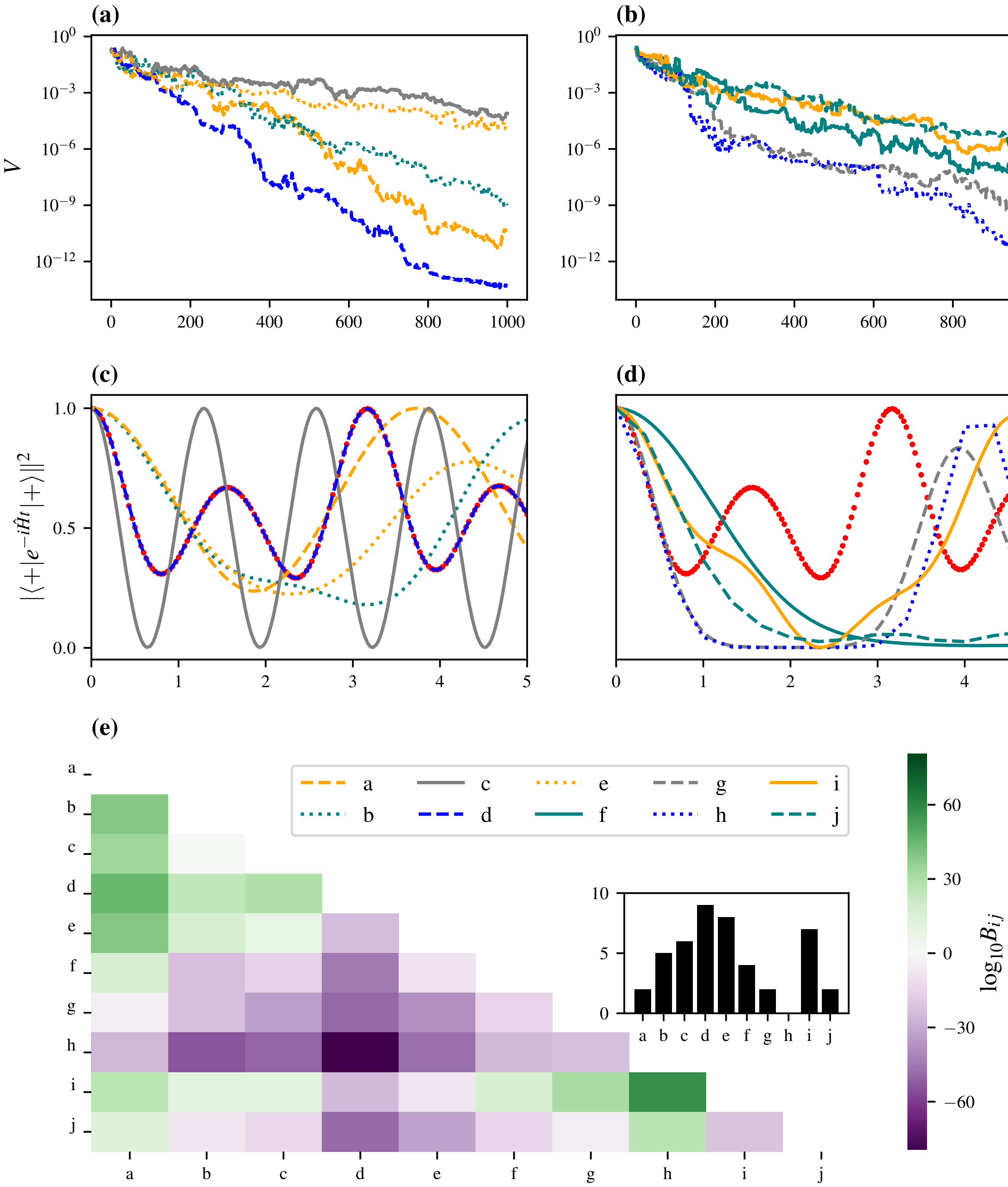

Figure 1.5: QMLA for set of lattices under Ising formalism. The lattice indices correspond to those in Fig. 1.1, and the true system is given by lattice d. (a,b) show the decrease in volume for each model's training phase. (spread over two plots for readibility) (c,d), trained models are used to reproduce dynamics, compared with the dynamics of the true system. (e) Heatmap of $\log_{10} B_{ij}$ between every pair of models. The BF is read as i versus j, where i is the model on the y-axis and j is the model on the x-axis. $\log_{10} B_{ij} > 0$ (green) favours the model listed on the y-axis; $\log_{10} B_{ij} < 0$ (purple) favours the model listed on the x-axis. The inset shows the number of BF comparisons won by each model, i.e. the models' scores. Implementation details are listed in Table A.1

through BF (Fig. 1.5**e**), and choosing the model which wins the largest number of BF contests. In this example, $\hat{H}_0$ is stronger than every alternative model according to the BFs, and is hence determined as $\hat{H}'$.

1.6 complete QMLA runs for lattice sets

In order to test QMLA robustly, we can use each of the lattices shown in Fig. 1.1 to specify $\hat{H}_0$, to ensure the algorithm is capable of finding the underlying model of arbitrary complexity, within the constraints of a prescribed model set[3]. Moreover, we can extend this test to the Heisenberg and Hubbard formalisms; note that due to the overhead given by the JWT (Section 1.4.1), i.e. the requirement of two qubits per site, we restrict study of the Hubbard model to lattices $a - e$ for practicality. By running 10 independent QMLA instances for each lattice under each formalism, we can gauge the success rate of the algorithm for distinguishing basic lattices from each other. We present the result of these tests in Fig. 1.6, finding in all cases that QMLA identifies $\hat{H}_0$ with success rates at least 70%.

We take this test case as evidence that the BF is a fair mechanism by which to distinguish between models. In general it will not be possible to prescribe the set of models to test, although this might serve as a straightforward mechanism for the calibration of quantum devices: suspected miscalibrations can be used in the design of such a set of models, along with a target $\hat{H}_0$ which the device should be able to implement. Then, by testing such a prescribed set and determining $\hat{H}'$, we can map the miscalibration between the intended and actual operations. In the ideal case, where it is mostly believed the device works, this application of QMLA may allow for fast, automated *verification* of the device: if QMLA finds $\hat{H}' = \hat{H}_0$ with high success given reasonable opportunity to miscompute, it may be sufficient verification that the device behaves as desired.

3 The remainder of this thesis is dedicated to cases where we do not prescribe the model set, but instead generate models dynamically.

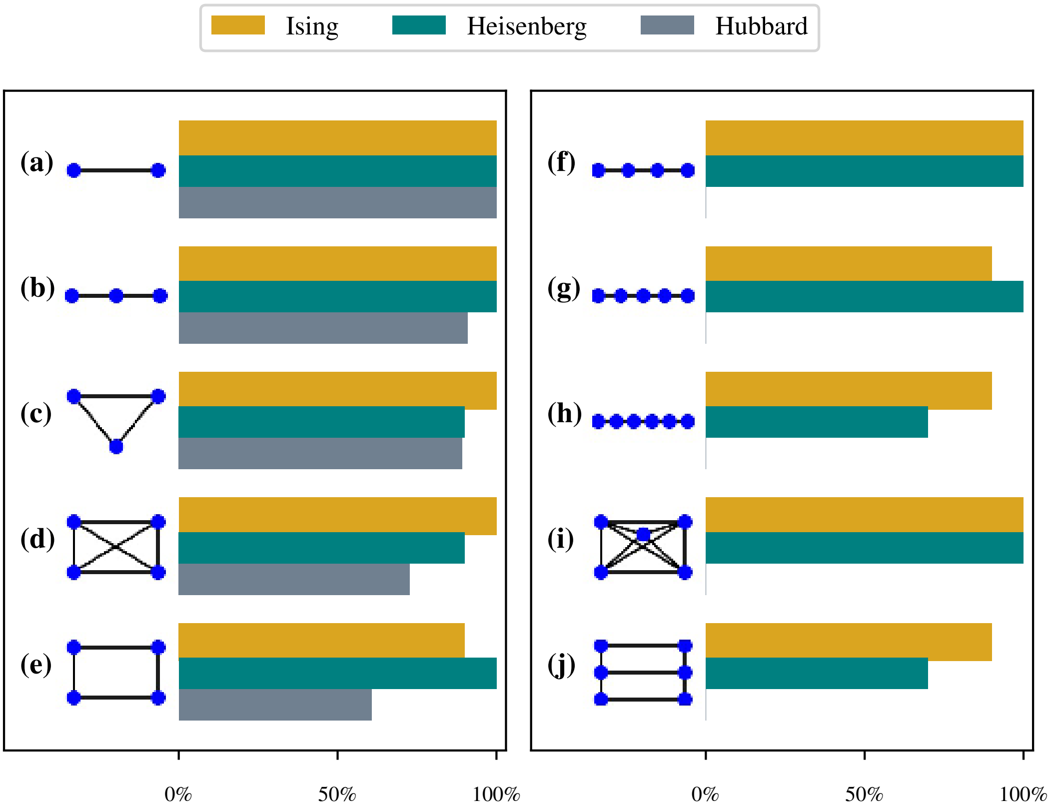

Figure 1.6: Rates of success for QMLA under various conditions. Each lattice is set as the true model $\hat{H}_0$ for ten independent instances. In each instance, the ES considers the available lattices (**a-j** for Ising and Heisenberg cases and **a-e** for the Hubbard case), and selects a champion model $\hat{H}'$ as that most consistent with data generated by $\hat{H}_0$. The figure displays the rate at which each lattice is correctly identified as $\hat{H}_0$ under standard Ising, Heisenberg and Hubbard formalisms. Implementation details are listed in Table A.1

2

BLACK BOX QUANTUM SYSTEMS

3 GENETIC ALGORITHMS

3.1 ADAPTATION TO QMLA FRAMEWORK

3.2 OBJECTIVE FUNCTIONS

3.3 APPLICATION

APPENDIX

A
FIGURE REPRODUCTION

Most of the figures presented in the main text are generated directly by the QMLA framework. Here we list the implementation details of each figure so they may be reproduced by ensuring the configuration in Table A.1 are set in the launch script. The default behaviour of QMLA is to generate a results folder uniquely identified by the date and time the run was launched, e.g. results can be found at the *results directory* qmla/Launch/Jan_01/12_34. Given the large number of plots available, ranging from high-level run perspective down to the training of individual models, we introduce a plot_level $\in \{1, ..., 6\}$ for each run of QMLA: higher plot_level informs QMLA to generate more plots.

Within the results directory, the outcome of the run's instances are stored, with analysis plots broadly grouped as

- evaluation: plots of probes and times used as the evaluation dataset.
- single_instance_plots: outcomes of an individual QMLA instance, grouped by the instance ID. Includes results of training of individual models (in model_training), as well as sub-directories for anlaysis at the branch level (in branches) and comparisons.
- combined_datasets: pandas dataframes containing most of the data used during analysis of the run. Note that data on the individual model/instance level may be discarded so some minor analyses can not be performed offline.
- exploration_strategy_plots plots specifically required by the ES at the run level.
- champion_models: analysis of the models deemed champions by at least one instance in the run, e.g. average parameter estimation for a model which wins multiple instances.
- performance: evaluation of the QMLA run, e.g. the win rate of each model and the number of times each term is found in champion models.
- meta analysis of the algorithm' implementation, e.g. timing of jobs on each process in a cluster; generally users need not be concerned with these.

In order to produce the results presented in this thesis, the configurations listed in Table A.1 were input to the launch script. The launch scripts in the QMLA codebase consist of many configuration settings for running QMLA; only the lines in snippet in Listing A.1 need to be set according to altered to retrieve the corresponding figures. Note that the runtime of QMLA grows quite quickly with N_E, N_P (except for the AnalyticalLikelihood ES), especially for the entire QMLA algorithm; running QHL is feasible on a personal computer in < 30 minutes for $N_e = 1000; N_p = 3000$.

```
#!/bin/bash
```

```
###############
# QMLA run configuration
###############
num_instances=1
run_qhl=1 # perform QHL on known (true) model
run_qhl_mulit_model=0 # perform QHL for defined list of models.
exp=200 # number of experiments
prt=1000 # number of particles

###############
# QMLA settings
###############
plot_level=6
debug_mode=0

###############
# Choose an exploration strategy
###############

exploration_strategy='AnalyticalLikelihood'
```

Listing A.1: "QMLA Launch scipt"

Figure	Exploration Strategy	Algorithm	N_E	N_P	Data
??	AnalyticalLikelihood	QHL	500	2000	Nov_16/14_28
Fig. 1.2	DemoIsing	QHL	500	5000	Nov_18/13_56
Fig. 1.3	DemoIsing	QHL	1000	5000	Nov_18/13_56
Fig. 1.4	DemoIsing	QHL	1000	5000	Nov_18/13_56
Fig. 1.5	IsingLatticeSet	QMLA	1000	4000	Nov_19/12_04
3*Fig. 1.6	IsingLatticeSet	QMLA	1000	4000	Sep_30/22_40
	HeisenbergLatticeSet	QMLA	1000	4000	Oct_22/20_45
	FermiHubbardLatticeSet	QMLA	1000	4000	Oct_02/00_09

Table A.1: Implementation details for figures used in the main text.

BIBLIOGRAPHY

[1] Ernst Ising. Beitrag zur theorie des ferromagnetismus. *Zeitschrift für Physik*, 31(1):253–258, 1925.

[2] Lars Onsager. Crystal statistics. i. a two-dimensional model with an order-disorder transition. *Physical Review*, 65(3-4):117, 1944.

[3] Stephen G Brush. History of the lenz-ising model. *Reviews of modern physics*, 39(4):883, 1967.

[4] Francisco Barahona. On the computational complexity of ising spin glass models. *Journal of Physics A: Mathematical and General*, 15(10):3241, 1982.

[5] Michael R Garey and David S Johnson. *Computers and intractability*, volume 174. freeman San Francisco, 1979.

[6] Andrew Lucas. Ising formulations of many np problems. *Frontiers in Physics*, 2:5, 2014.

[7] Giuseppe E Santoro and Erio Tosatti. Optimization using quantum mechanics: quantum annealing through adiabatic evolution. *Journal of Physics A: Mathematical and General*, 39(36):R393, 2006.

[8] Victor Bapst, Laura Foini, Florent Krzakala, Guilhem Semerjian, and Francesco Zamponi. The quantum adiabatic algorithm applied to random optimization problems: The quantum spin glass perspective. *Physics Reports*, 523(3):127–205, 2013.

[9] Mark W Johnson, Mohammad HS Amin, Suzanne Gildert, Trevor Lanting, Firas Hamze, Neil Dickson, Richard Harris, Andrew J Berkley, Jan Johansson, Paul Bunyk, et al. Quantum annealing with manufactured spins. *Nature*, 473(7346):194–198, 2011.

[10] Walter Greiner, Ludwig Neise, and Horst Stöcker. *Thermodynamics and statistical mechanics*. Springer Science & Business Media, 2012.

[11] John Hubbard. Electron correlations in narrow energy bands. *Proceedings of the Royal Society of London. Series A. Mathematical and Physical Sciences*, 276(1365):238–257, 1963.

[12] Richard T Scalettar. An introduction to the hubbard hamiltonian. *Quantum Materials: Experiments and Theory*, 6, 2016.

[13] Editorial. The hubbard model at half a century. *Nature Physics*, 2013.

[14] Pascual Jordan and Eugene Paul Wigner. über das paulische äquivalenzverbot. In *The Collected Works of Eugene Paul Wigner*, pages 109–129. Springer, 1993.

[15] Mark Steudtner and Stephanie Wehner. Fermion-to-qubit mappings with varying resource requirements for quantum simulation. *New Journal of Physics*, 20(6):063010, 2018.

[16] Jarrod McClean, Nicholas Rubin, Kevin Sung, Ian David Kivlichan, Xavier Bonet-Monroig, Yudong Cao, Chengyu Dai, Eric Schuyler Fried, Craig Gidney, Brendan Gimby, et al. Openfermion: the electronic structure package for quantum computers. *Quantum Science and Technology*, 2020.